Coverage and Stability of NH_x Terminated Cobalt and Ruthenium Surfaces: a First Principles Investigation

Ji Liu[a] and Michael Nolan[a,*]

[a] Tyndall National Institute, University College Cork, Lee Maltings, Dyke Parade, Cork, T12 R5CP, Ireland

Corresponding author:

[*]E-mail: Michael.nolan@tyndall.ie. Tel: +353 021 2346983

Abstract

In the atomic layer deposition (ALD) of Cobalt (Co) and Ruthenium (Ru) metal using nitrogen plasma, the structure and composition of the post N-plasma NH_x terminated (x = 1 or 2) metal surfaces are not well known but are important in the subsequent metal-containing pulse. In this paper, we use the low-index (001) and (100) surfaces of Co and Ru as models of the metal polycrystalline thin films. The (001) surface with a hexagonal surface structure is the most stable surface and the (100) surface with a zigzag structure is the least stable surface but has high reactivity. We investigate the stability of NH and NH_2 terminations on these surfaces to determine the saturation coverage of NH_x on Co and Ru. NH is most stable in the hollow hcp site on (001) surface and the bridge site on the (100) surface, while NH_2 prefers the bridge site on both (001) and (100) surfaces. The differential energy is calculated to find the saturation coverage of NH and NH_2. We also present results on mixed NH/NH_2-terminations. The results are analyzed by thermodynamics using Gibbs free energies (ΔG) to reveal temperature effects on the stability of NH and NH_2 terminations. Ultra-high vacuum (UHV) and standard ALD operating conditions are considered. Under typical ALD operating conditions we find that the most stable NH_x terminated metal surfaces are 1 ML NH on Ru (001) surface (350K-550K), 5/9 ML NH on Co (001) surface (400K-650K) and a mixture of NH and NH_2 on both Ru (100) and Co (100) surfaces.

1. *Introduction*

With the downsizing of semiconductor devices, the copper interconnect becomes the key challenge and the volume available in the via is reduced.[1-3] Barrier and liner layers are needed to prevent copper diffusion and to promote copper adhesion or wetting. Future developments in this area envisage replacing copper with metals such as Co or Ru which have lower resistivity at typical device dimensions. Co can be used as a seed layer for metallization of interconnects and Ru is a potential electrode material for DRAM capacitors and MOSFETs.[4] In modern device structures, the barrier and liner layers and the interconnect require high conformality and continuous thin film deposition at the atomic scale. Atomic layer deposition (ALD) is the leading technique for depositing thin films with these properties in semiconductor technology.[5,6] ALD usually consists of two half-cycle reactions that are each self-limiting with a purge after each step. The reactions stop when all available surface sites are consumed and this self-limiting property can ensure, at least in principle, that the thickness of the deposited thin film is precisely controlled by changing the number of cycles.[7,8] ALD is used in depositing metal oxides[9-11] (e.g. TiO_2), metal nitride[12] (e.g. TaN), and metals[13,14] (e.g. Cu).

Plasma enhanced ALD (PE-ALD) is a variant of ALD that allows low-temperature deposition, which can make the ALD process consistent with the permitted processing temperatures in semiconductor device fabrication.[15] The plasma source can be oxygen or nitrogen. The O-plasma mechanism has been well-established in recent years.[16-19] The oxygen reactant can be H_2O, O_3, or H_2O_2 to promote metal oxide ALD growth.[20,21] Hydroxylated (OH-terminated) surfaces are produced after this pulse[22,23] and hydroxylated metal oxide surfaces have been widely studied both for the ALD process[7,9,10] and in catalysis for reactions including water-gas shift and photocatalysis[24-26].

However, by contrast, the N-plasma mechanism is not well understood. In particular, the nature and stability of NH_x terminated metal surfaces that would be produced during the N-plasma deposition and required for modelling the N-plasma ALD process are entirely lacking. When depositing metals, such as Co and Ru, the use of N-plasma is preferred because this avoids oxygen contamination and subsequent oxidation of the metal surface. Previous studies have used ammonia adsorption or decomposition on platinum group metal surfaces including Pt, Pd and Rh[27,28] or hexagonal close-packed (hcp) metal surfaces such as Ru[29,30] in catalysis-focused studies. The nature of the most stable NH_x fragment on these metals varies with different surface orientations and the decomposition is structure sensitive.

The ALD of Co uses metal organic precursors such as cyclopentadienyl dicarbonyl cobalt ($CoCp(CO)_2$) and bis-cyclopentadienyl cobalt ($CoCp_2$)[31-33] and the other precursors are NH_3 or a mixture of N_2 and H_2. The first ALD of Ru used $RuCp_2$ and O_2 as precursors. The reported main byproducts are CO_2 and H_2O. A combination of high O_2 dose and low Ru precursor dose can result in RuO_2 rather than Ru.[4] Other Ru precursors such as $Ru(EtCp)_2$ and $CpRu(CO)_2Et$ have also been developed.[34,35] Generally, the deposition temperature is above 200 °C for these metal organic precursors.[36,37] As pointed out earlier, oxygen can oxidize metal surface and use of N-plasma is therefore important for the deposition of metals. Experimental results have pointed out that both NH_3-plasma and N_2/H_2 plasma can result in high purity and low resistivity Co thin film. However, H-plasma alone or separate N_2 and H_2 plasma can produce lower purity and higher resistivity Co thin films.[32,33,38] It has been argued that the NH_x-terminated metal surfaces play an important role in Co thin film deposition.[32,39] However, the nature of the NH_x-terminated metal surfaces is not yet understood and this is the key advance in our present work.

Density functional theory (DFT) calculations have successfully applied to reveal the reaction mechanism of O-plasma in PE-ALD.[40-42] However, limited theoretical studies are available that discuss N-plasma PE-ALD.[43] Delabie *et al.*[44,45] have simulated the ALD of Ru on Ru

surfaces focusing on Ru precursor reactions with bare Ru surface and H-terminated Ru surfaces. The effect of nitrogen plasma is not considered in that paper. A full ALD cycle is as follows - starting from the post N-plasma cycle, the metal surface will be NH_x-terminated surface, where *x* can be 1 or 2. Then the metal precursors ($RuCp_2$ and $CoCp_2$) are adsorbed on the NH_x-terminated metal surfaces and a hydrogen transfer step can produce CpH which desorbs. The second half reaction with N-plasma produces a deposited metal layer with an NH_x-terminated surface. A whole cycle is completed and the surface is ready for the next cycle. The present paper is focused on using first principles simulations to identify stable NH_x-terminated Co and Ru surfaces by considering termination of Co and Ru with amine (NH_2) or imine (NH) species and mixed termination with NH_2 and NH. The results are further analyzed with ab initio thermodynamics using the Gibbs energy (ΔG) in which the effect of temperature and pressure is considered. The results show that under ALD operating condition, the nature of the NH_x terminated Co and Ru surfaces can be strongly dependent on the temperature at a given pressure. For example, 1ML NH is preferred on the Ru (001) surface for a temperature range between 350K and 550K and 5/9 ML NH is preferred on Co (001) surface for temperature range between 400K and 650K. On the (100) surfaces, the unique trench structure allows the surface coverage to be up to 2 ML. Starting with 9NH and $9NH_2$, NH is desorbed from surface gradually to produce 6NH and $9NH_2$ as the temperature increases. Similarly, NH_2 can be desorbed to produce 6NH and $6NH_2$ (0.67 ML coverage) on Co or Ru surfaces. The metal surface terminations would affect the precursor reaction during the ALD process. The study on NH_x terminated metal surface is vital and essential to investigate the PE-ALD deposition of metal thin films.

2. *Methods and Computational Details*

All the calculations are performed on the basis of spin-polarized DFT with the projector augmented wave (PAW) formalism[46], as implemented in the Vienna *ab* initio simulations package (VASP 5.3) code. The generalized gradient approximation (GGA) with the parameterization of Perdrew-Burke-Ernzerhof (PBE) is used for the exchange-correlation functional.[47,48] The energy cutoff is set to be 400 eV for the plane wave expansion. The convergence of energy and forces are set to be 1×10^{-4} eV and 0.01eV/□, respectively. The bulk Co and Ru crystal structure is optimized by simultaneously relaxing the ionic positions, cell volume and cell shape at a higher plane wave energy cutoff of 550eV and a Monkhorst-Pack grid[49] k-point mesh of 12 × 12 × 6. The resulting lattice constants are a = b = 2.489Å, and c = 4.035Å for Co bulk and a = b = 2.715Å, and c = 4.285Å for Ru bulk.

The deposited Co or Ru films by ALD are polycrystalline and have random surface orientations after low temperature deposition. The Ru crystallite tends to orient towards [001] direction at elevated temperature or increased plasma power.[4] In this paper, three X-ray detected low-index surfaces (001), (100), and (101) are considered. The surface models consist of multi-layer Ru or Co and the vacuum region is up to 15 Å. Both (3 × 3) and (4 × 4) surface supercell expansions are considered to minimize the neighboring effect of adsorbates (NH and NH_2). The bottom three layers are fixed during the calculations. The configurations of these surfaces are shown in Figure 1 and the calculated properties are listed in Table 1.

Both Ru and Co have the lowest surface energy along [001] direction, which forms a hexagonal structure and is the most stable surface. The (100) surface has a zigzag structure and shows high reactivity, while the (101) surface is a nearly flat surface with surface energy in between (001) and (100) surfaces. Based on the surface stability and reactivity, we have chosen the most

stable (001) surface and the least stable, and high reactivity surface, (100) to study the stability of NH_x-terminations.

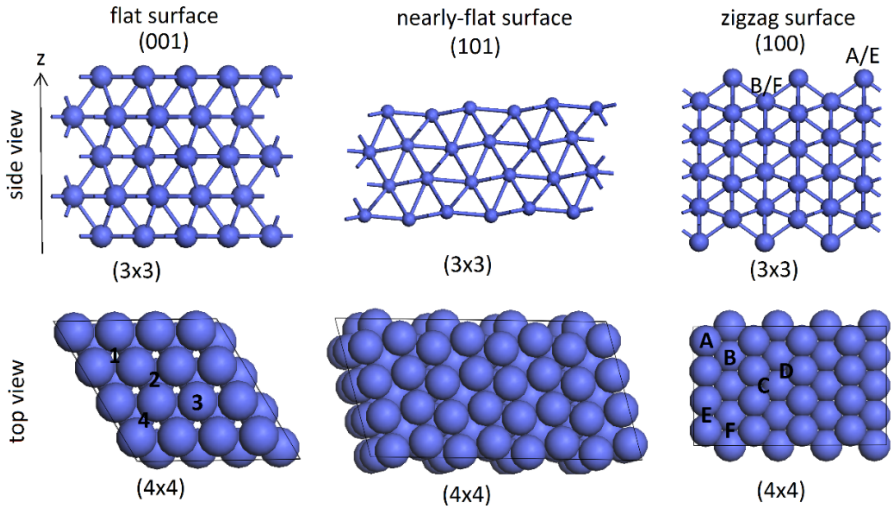

Figure 1. The top and side view of Ru or Co surfaces in three orientations: (001), (101), and (100). The adsorption sites on (001) surfaces are highlighted as 1 (fcc), 2 (hcp), 3 (top), and 4 (bridge); The adsorption sites on (100) surfaces are highlighted as A, B (top), C, D (hollow), and E, F (bridge).

The stability of NH_x terminations is defined by the formula:

$$E_{ad} = E_{tot} - E_{slab} - E_A,$$

where E_{tot}, E_{slab}, and E_A are the energy of the metal slab with termination *A* (*A* = NH, NH_2), an isolated slab model for the clean metal surface, and isolated adsorbate *A*, respectively. The reference energy for the adsorbate can be computed using $\frac{1}{2}(N_2+H_2)$ and $\frac{1}{2}N_2+H_2$, for NH and NH_2, respectively. These correspond to typical gases in the nitrogen plasma set-up. These computed energies can be thought of as an indication of how an NH_x termination resists desorption with temperature, which would be probed through a temperature programmed desorption experiment. The activation barriers reported in this paper are computed using

climbing image nudged elastic band (CI-NEB) method[50] with 6 images including the starting and ending geometries and with force converged to 0.01eV/□.

Table 1. The calculated properties of low index surfaces of Co and Ru.

Ru_slab											
3×3	Surf. Area (nm^2)	E_surf (J/m^2)	No. of atom	No. of layer	k-points	4×4	Surf. Area (nm^2)	E_surf (J/m^2)	No. of atom	No. of layer	k-points
Ru_100	1.05	3.33	45	5	3×2×1	Ru_100	1.86	3.36	80	5	2×1×1
Ru_001	0.66	2.29	45	5	3×3×1	Ru_001	1.18	2.31	80	5	2×2×1
Ru_101 (2×4)	1.10	2.93	64	8	2×2×1	Ru_101	2.20	2.71	128	8	1×2×1
Co_slab											
3×3						4×4					
Co_100	0.90	2.69	45	5	3×2×1	Co_100	1.61	2.69	80	5	2×1×1
Co_001	0.56	1.85	45	5	3×3×1	Co_001	0.99	1.88	80	5	2×2×1
Co_101	1.06	2.45	72	8	1×1×1	Co_101	1.89	2.27	128	8	1×1×1

3. *Results and Discussions*

3.1 Structure and Stability of NH or NH_2 species at Co and Ru Surfaces

To begin with, we have considered the termination of Co and Ru (001) and (100) surfaces with single NH or NH_2 species to assess the preferred binding sites. The possible adsorption sites are shown in Figure 1. For the (001) surfaces, four adsorption sites including hcp, fcc, bridge, and top are considered. On the (100) surface six possible sites are considered, which are top (A and B), hollow (C and D), and bridge (E and F). Due to the unique trench structure of the (100) surface, sites A and E are located on the surface, while site B and F are anchored to zigzag channel. The calculated energies of NH and NH_2 adsorption, relative to $\frac{1}{2}(N_2+H_2)$ and $\frac{1}{2}N_2+H_2$, respectively, are listed in Table 2; to facilitate the discussion, we also align the adsorption energy of the most stable site to be zero as a reference to discuss the stability of NH_x terminations.

The configurations of the most stable single NH and NH_2 terminations on Ru and Co surfaces are shown in Figure 2 and Figure 3, respectively. We see that the most stable binding sites are the same on each surface facet. On the (001) surface, NH prefers to bind on the hcp site while NH_2 prefers to bind on a bridge site. On the (100) surface, both NH and NH_2 prefer the bridge site and these are the bridge F (zigzag channel) for NH and bridge E (surface) for NH_2. A larger surface supercell expansion ((4 × 4) supercell) does not affect the most stable sites and these results are consistent with a previous modelling report on NH_3 synthesis.[29,51] After relaxation, NH is in an upright position with the nitrogen atom adsorbed on hollow site on (001) surfaces or bridge site on (100) surfaces. The nearest metal-N distances are 1.855□ and 1.889□ on Co (001) and Co (100) surfaces and 2.012□ and 2.247□ on Ru (001) and Ru (100) surfaces, respectively. NH_2 is also in an upright position with the nitrogen atom binding to bridge site. The nearest metal-N distances are 1.975□ and 1.950□ on Co (001) and Co (100) surfaces and

Table 2. The calculated adsorption energies of NH and NH_2 on Co and Ru (001) and (100) surfaces. The energies in bracket are with respect to the energy of most stable site.

Adsorption energy/eV									
NH		Co(001) 3×3	Co(001) 4×4	Ru(001) 3×3	Ru(001) 4×4	NH		Co(100) 3×3	Ru(100) 3×3
	hcp	-3.68 (0.00)	-3.61 (0.00)	-3.74 (0.00)	-3.68 (0.00)		top_A	-2.29 (1.41)	2.02 (1.56)
	bridge	-2.75 (0.93)	-3.14 (0.48)	hollow*	hollow*		top_B	-2.12 (1.58)	-2.49 (1.09)
	top	-1.27 (2.41)	-0.64 (2.97)	-1.78 (1.96)	-1.73 (1.95)		hollow_C	1.68 (5.38)	top*
	fcc	-3.21 (0.47)	-3.17 (0.44)	-3.36 (0.38)	-3.34 (0.34)		hollow_D	0.96 (4.66)	bridge*
							bridge_E	-3.22 (0.48)	-3.30 (0.28)
							bridge_F	-3.70 (0.00)	-3.58 (0.00)
NH_2						NH_2			
	fcc	bridge*	bridge*	bridge*	-3.65 (0.92)		top_A	-2.88 (1.42)	-2.51 (1.53)
	bridge	-3.37 (0.00)	-3.39 (0.00)	-3.64 (0.00)	-4.57 (0.00)		top_B	-3.63 (0.66)	-3.34 (0.70)
	top	-3.23 (0.14)	2.83 (0.56)	-2.98 (0.66)	-1.94 (2.63)		hollow_C	-3.54 (0.75)	-3.32 (0.72)
							hollow_D	bridge*	bridge*
							bridge_E	-4.29 (0.00)	-4.04 (0.00)
							bridge_F	-3.27 (1.02)	-2.76 (1.28)

*: after structure relaxing, the NH or NH_2 diffuse to * site from the initial site.

2.104□ and 2.097□ on Ru (001) and Ru (100) surfaces, respectively. We have calculated the partial density of states (PDOS) and they are shown in Figure 4 and Figure 5. We see that there is hybridization between the 2*p*-orbitals of nitrogen and *d*-orbitals of Co or Ru atom. The PDOS looks quite similar for the same adsorbate on Co or Ru surfaces.

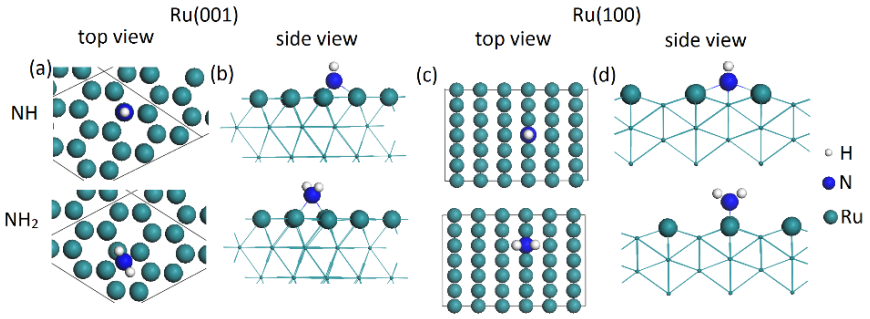

Figure 2. The configurations of the most stable adsorption of NH and NH_2 on Ru (001) and (100) surfaces including top view and side view.

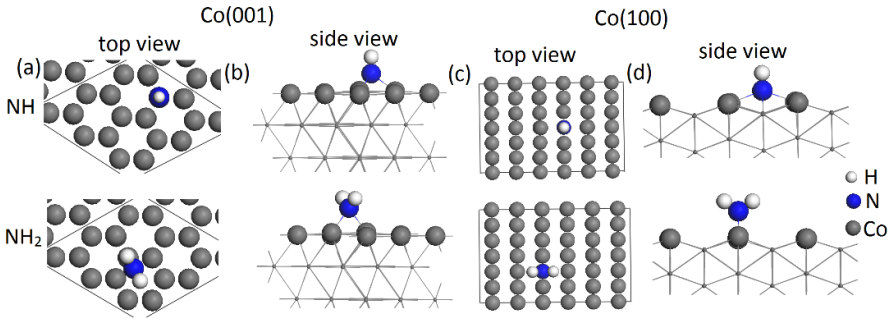

Figure 3. The configurations of the most stable adsorption of NH and NH_2 on Co (001) and (100) surfaces including top view and side view.

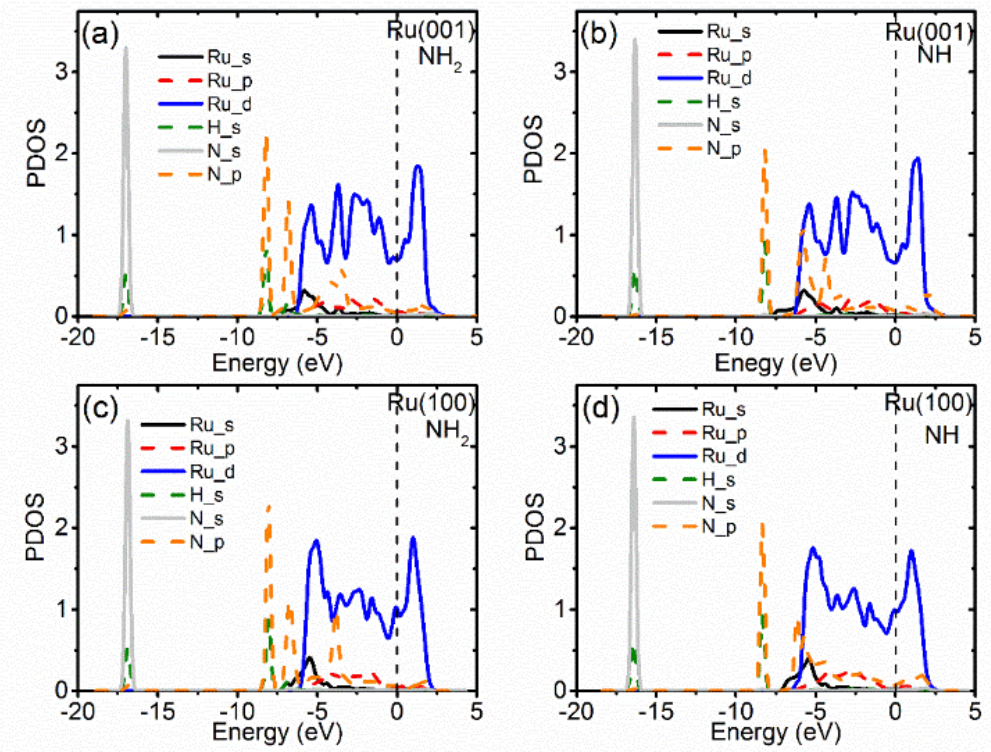

Figure 4. The plotted partial density of states (PDOS) of NH and NH_2 on Ru (001) and (100) surfaces at the most stable adsorption site.

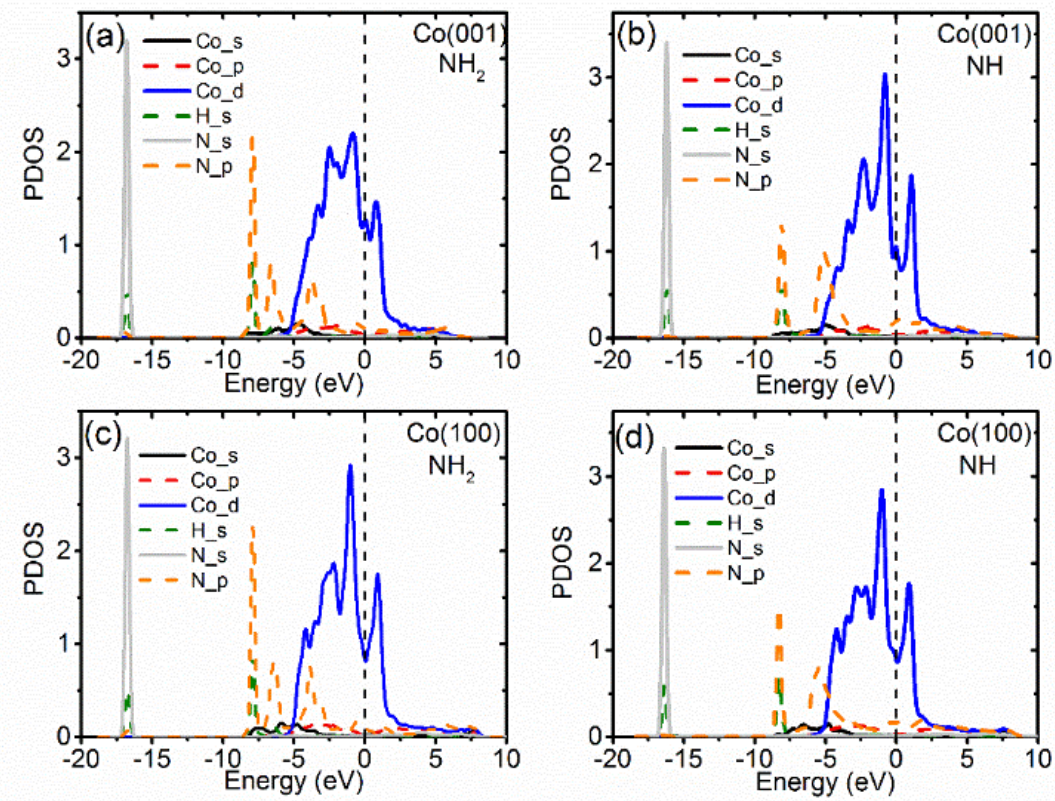

Figure 5. The plotted partial density of states (PDOS) of NH and NH_2 on Co (001) and (100) surfaces at the most stable adsorption site.

3.2 Coverage Dependence of the Stability of NH_x Terminations on Ru and Co Surfaces

Once the stable adsorption sites for single NH and NH_2 species are confirmed, we further investigate the stability of different surface coverages by increasing the number of adsorbates one by one in (3 × 3) unit cell. The differential energy is defined as

$$\Delta E = E_{(n+1)A} - E_{nA} - E_A,$$

where $E_{(n+1)A}$ and E_{nA} are the energies of (n+1) *A* species on the metal surface and n *A* species on the metal surface, respectively. The reference energy for adsorbate *A* is as previously described. This differential energy is used to find the saturation coverage, where a positive

differential energy means that further NH or NH_2 species cannot be accommodated on the metal surface and we are at the saturation coverage. The calculated adsorption and differential energies with respect to surface coverage are plotted in Figure 6 and Figure 7, respectively. NH and NH_2 have similar stability on both (001) surfaces, while on the (100) surfaces, NH_2 is clearly more stable than NH for all coverages. The structure of the (100) surfaces with the larger metal-metal distance and the trench appears to be able to accommodate the NH_2 species. Considering the differential energy, on the (001) surfaces, the calculated differential energies deviate from linearity and/or become positive at a coverage that depends on the identity of the surface. This deviation means that adding another NH or NH_2 to the surface is no longer favorable at this coverage and the effect of this is the desorption of NH or NH_2 from the metal surfaces, which we find leads to the formation of N_2H_2 when starting from NH or NH_2 terminations with high coverages. This allows us to then determine the most stable coverage of NH and NH_2 on all surfaces.

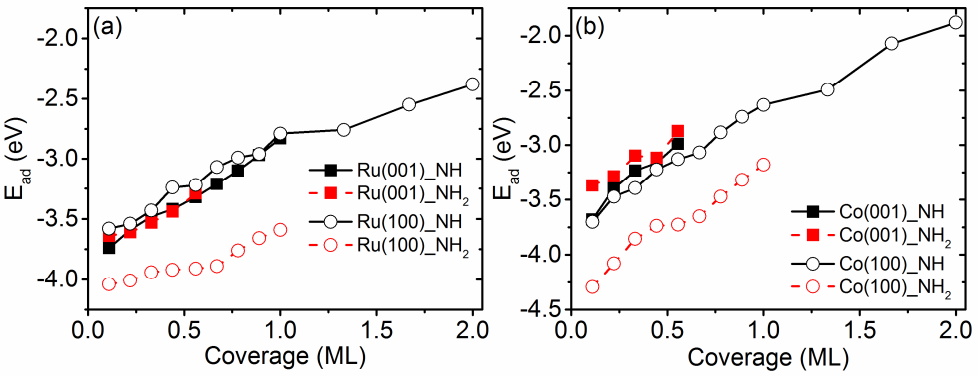

Figure 6. The calculated adsorption energies of NH and NH_2 on Co and Ru (001) and (100) surfaces.

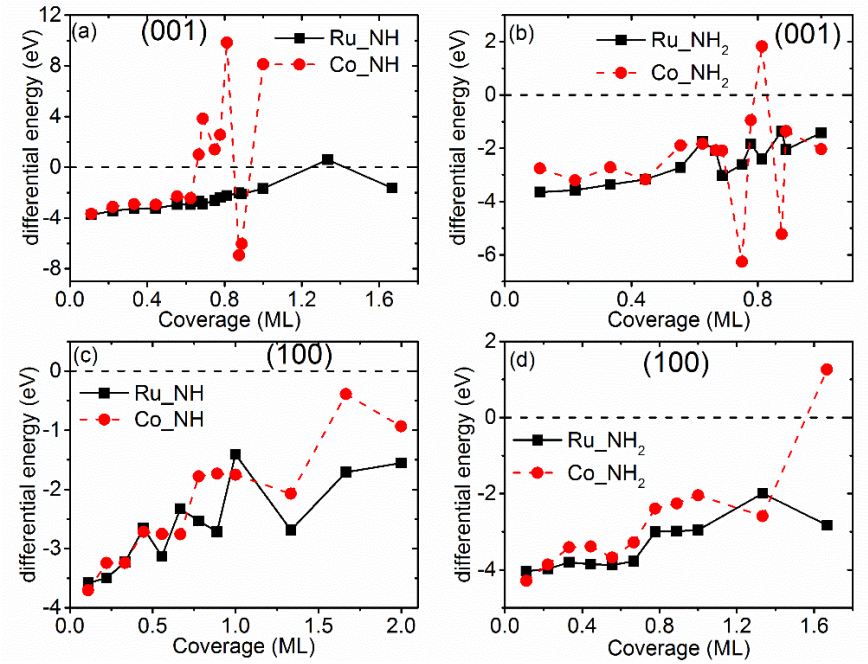

Figure 7. The calculated differential energy of NH and NH_2 on Co and Ru surfaces as a function of coverage. (a) (001)-NH terminated, (b) (001)-NH_2 terminated, (c) (100)-NH-terminated and (d) (100)-NH_2-terminated. A positive energy means that further addition of NH or NH_2 is not favourable and therefore under high coverages, NH and NH_2 would desorb from surface and NH_2 may dissociate into NH.

For example, on the Co (001) surface, covering the surface with 1 ML NH species releases two N_2H_2 molecules structure upon relaxing to give a maximum coverage of 5/9 ML. In order to understand further the interaction between molecules under high coverage and check for size effects, the surface supercell size was increased to a (4 × 4) supercell with the number of adsorbed species ranging from 9 (9/16 ML) to 14 (14/16 ML). After relaxing this structure, we find desorption of pairs of NH molecules as N_2H_2 from the Co (001) surface due to the repulsion between neighboring NH species which confirms the instability of the full coverage of NH on Co (001).

In addition to desorption, we also find that adsorbed NH_2 species can dissociate into NH and H or form NH_3 on both Co and Ru surfaces under high coverage, which shows that NH_2 is quite unstable under high coverage. The barrier for dissociation of NH_2 to NH and H on the Ru(001) surface was computed as 0.71eV in a previous DFT study.[51] We have calculated the dissociation barrier for NH_2 dissociation to NH and H on the Co (001) surface using the CI-NEB method and the calculated barrier is 0.71eV, which will be easily overcome at typical ALD operating temperatures. This is consistent with a previous report that focused on NH_3 synthesis,[29,51] and found that NH_2 is difficult to form but relatively easy to dehydrogenate due to high formation barrier (1.28eV) but relatively low dehydrogenation barrier (0.71eV). Additionally, as pointed out in the same report, the reaction barrier would decrease as the surface coverage increases. Our finding of NH_2 instability at high coverages supports this finding as we observe spontaneous dissociation of NH_2.

From the computed energies, the saturation coverage of NH on Co (001) surface is predicted to be 5/9 ML, while on Ru (001) surface full coverage of 1 ML is stable. This difference between the two metals arises from the larger Ru (001) surface lattice (Ru lattice constant is 2.715Å and Co lattice constant is 2.489Å) and the resulting larger Ru-Ru distance when compared to the Co (001) surface; the Ru-Ru distance is 2.716□ and the Co-Co distance is 2.479□. Thus, the repulsion between NH groups will be weaker on the Ru (001) surface, as a result of the longer N-N distance; this distance is 1.245□ on Co and 1.358□ on Ru. The saturation coverage of NH_2 on both Ru and Co (001) surfaces is 5/9 ML, so here the structural features of the metal surfaces play no role in determining the stability.

On (100) surfaces of Ru and Co, the saturation coverage of NH can be up to 2 ML; this arises since after occupying the initially preferred channel bridge site, NH will continue be adsorbed on the surface bridge site until full coverage is achieved on the zigzag surface. The saturation coverage of NH_2 on Ru and Co (100) surfaces is 1 ML. After occupying the surface bridges,

additional NH_2 adsorbed on channel bridge site desorb from surface during the relaxation. The calculated saturation coverages are summarized in Table 3. The configurations of the saturated adsorption of NH_x fragments are shown in Figure 8 and Figure 9.

Table 3. The calculated individual saturation coverage of NH and NH_2 on Co and Ru (001) and (100) surfaces.

	Ru		Co	
	(001)	(100)	(001)	(100)
NH	1ML	2ML	5/9ML	2ML
NH_2	5/9ML	1ML	5/9ML	1ML

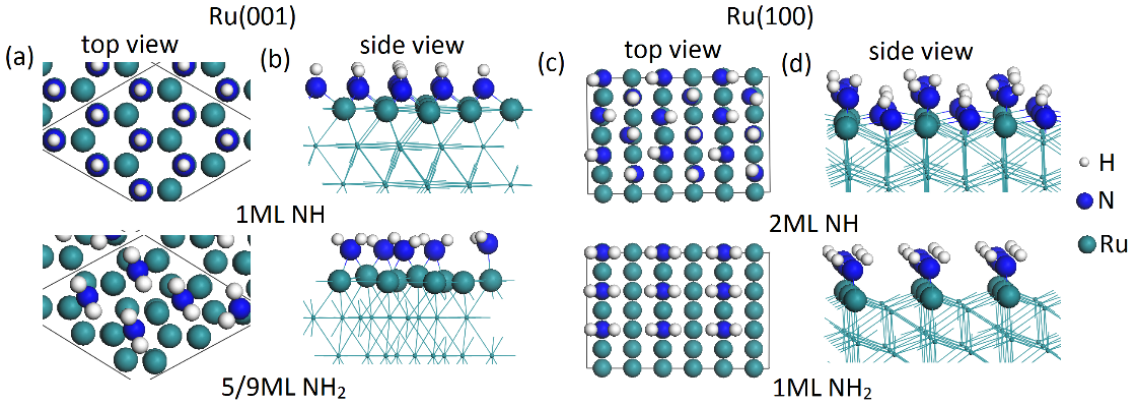

Figure 8. The configurations of the saturated adsorption of NH and NH_2 on Ru (001) and (100) surfaces including top view and side view.

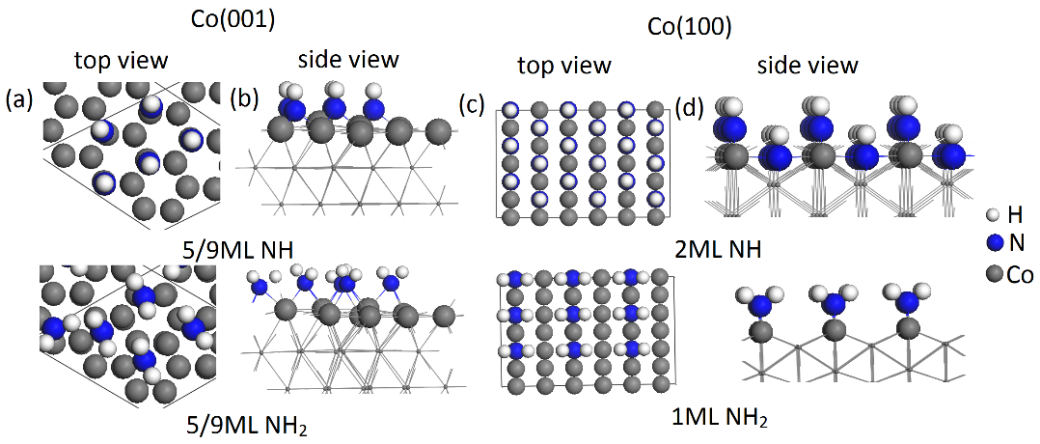

Figure 9. The configurations of the saturated adsorption of NH and NH_2 on Co (001) and (100) surfaces including top view and side view.

3.3 Termination with Mixed NH and NH_2 Species.

We now consider the termination of the Co and Ru surfaces with a mix of NH and NH_2 species to investigate the stability of mixed NH and NH_2-terminated surfaces. On the (001) surfaces, due to the instability of adsorbed NH_2 at high coverage, an NH terminated surface model is used in the simulation of mixed NH/NH_2 termination.

On the (100) surfaces, an NH_2 terminated surface model is used in the simulation of the mixed NH/NH_2 termination as a result of the greater stability of NH_2 compared to NH. All the calculations for the mixed termination cases are performed with the (3 × 3) surface supercell. For the Ru (001) surface, the NH saturation coverage is up to 1ML, and additional NH_2 desorbs from surface upon relaxation. Thus, Ru (001) is excluded from further discussion and will not show mixed termination with NH and NH_2.

For Co (001), the saturation coverage of NH is 5/9 ML and starting from this coverage, NH_2 species are adsorbed on the available surface sites one by one until reaching full coverage. For Ru (100) and Co (100), since the NH_2 saturation coverage is up to 1 ML, we have considered

two NH_2 terminated models: $6NH_2$ and $9NH_2$ on (3 × 3) surface. Due to the stability of the NH termination, we set the number of surface NH to be 3, 6 or 9 instead of increasing the coverage of NH species one by one. These models and the energies of the mixed terminations are presented in Table 4.

Table 4. The mixed termination models and adsorption energies on Co (001) surface and (100) surfaces. The adsorption energies in the bracket are with reference to pre-covered NH or NH_2 models.

Adsorption energy/eV				
Co(001)			Ru(100)	Co(100)
$5NH+NH_2$	-2.72 (-1.35)	$6NH_2+6NH$	-3.16 (-3.24)	-2.89 (-2.72)
$5NH+2NH_2$	-2.57 (-1.51)	$6NH_2+9NH$	-2.87 (-3.00)	-2.65 (-2.67)
$5NH+3NH_2$	-2.14 (-0.73)	$9NH_2+3NH$	-3.24 (-2.20)	-2.82 (-1.76)
		$9NH_2+6NH$	-3.02 (-2.17)	-2.64 (-1.83)
		$9NH_2+9NH$	-2.74 (-2.70)	-2.43 (-2.23)

On all surfaces, the energy gain per adsorbate generally decreases with increasing the number of adsorbate species. On the (001) surfaces, the surface cannot reach full coverage (1ML, in total 9 adsorbates) due to the competition between NH and NH_2 and Co (001) shows a maximum of $5NH + 3NH_2$. On the (100) surface, full coverage of mixed NH and NH_2 (2 ML, with 18 adsorbed species) is possible. This is due to the unique zigzag surface structure, which provides more available sites over a larger surface area.

3.4 Thermodynamics

NH and NH_2 prefer to bind on different adsorption sites on Co and Ru surfaces. The competition between NH and NH_2 terminations can be more deeply analysed from ab initio thermodynamics. The Gibbs free energy (ΔG) is calculated to extend the results of DFT by adding the effect of temperature and pressure. Two values of the pressure are selected. One is the ultra-high vacuum (UHV) condition ($P/P^o = 5\times10^{-14}$) and the second is the standard ALD operating condition, taken from ref. [32] ($P/P^o = 1.97\times10^{-6}$); P^o is the standard pressure, i.e. 1 atm. For the adsorption on metal surface, the ΔG is calculated by the equation (1):

$$\Delta G = G\left[{metal}/{total}\right] - G[metal] - G_{gas}(adsorbate) \quad (1)$$

The G[metal/total], G[metal], and G_{gas}(adsorbate) are the Gibbs free energy of the metal surface (Co or Ru) with terminating groups (NH or NH_2), the clean metal, and the gas phase reference molecules (N_2 and H_2), respectively. The contribution of vibrations to the solid surface is negligible and can be substituted by the results from DFT.[52] The gas phase term can be calculated by the equation (2):

$$G_{gas}(adsorbate) = E_{DFT} + \mu(T, P^o) + k_B T ln\left({P}/{P^o}\right) \quad (2)$$

E_{DFT} is the DFT total energy, μ is the chemical potential at different temperatures and can be obtained from thermodynamic tables, and the last term is the contribution of the temperature and adsorbate partial pressure. In this work, the energy of NH and NH_2 are determined with reference to ½(N_2+H_2) and ½N_2+H_2, respectively. Experimentally, the typical ALD deposition temperature is in the range of 350K to 650K for metal organic precursors.[4,13,39] The plotted Gibbs free energy for the two pressures considered, namely typical ALD operating pressure and ultra-high vacuum (UHV) condition are shown in Figure 10 and Figure 11, respectively.

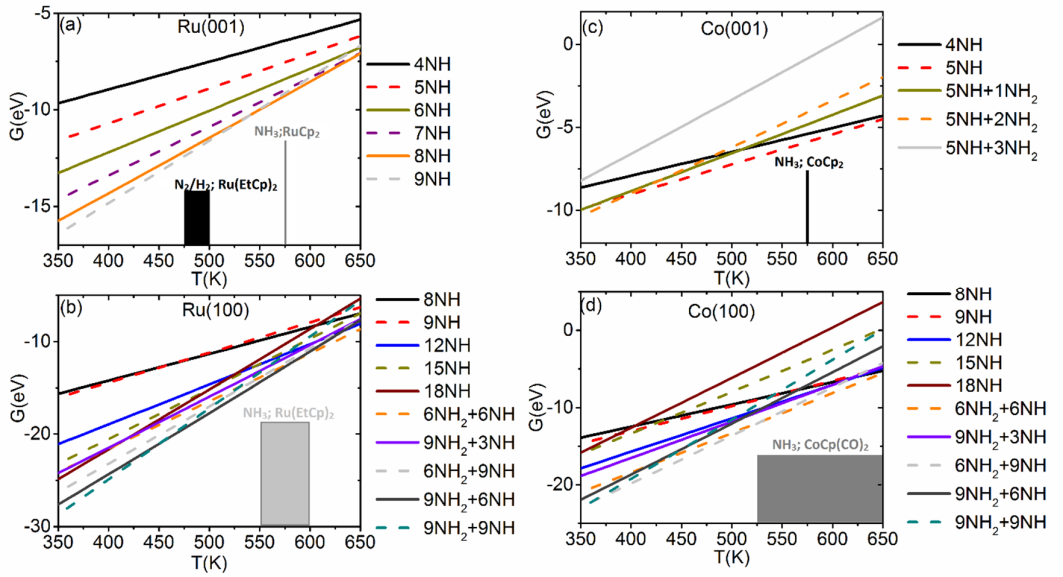

Figure 10. The plotted Gibbs free energy (ΔG) of NH_x with respect to operating temperature on Ru and Co surfaces. The pressure is set to be ALD operating condition ($P/P^o = 1.97\times10^{-6}$). The inserts show the experimentally reported deposition temperatures taken from Ref.4.

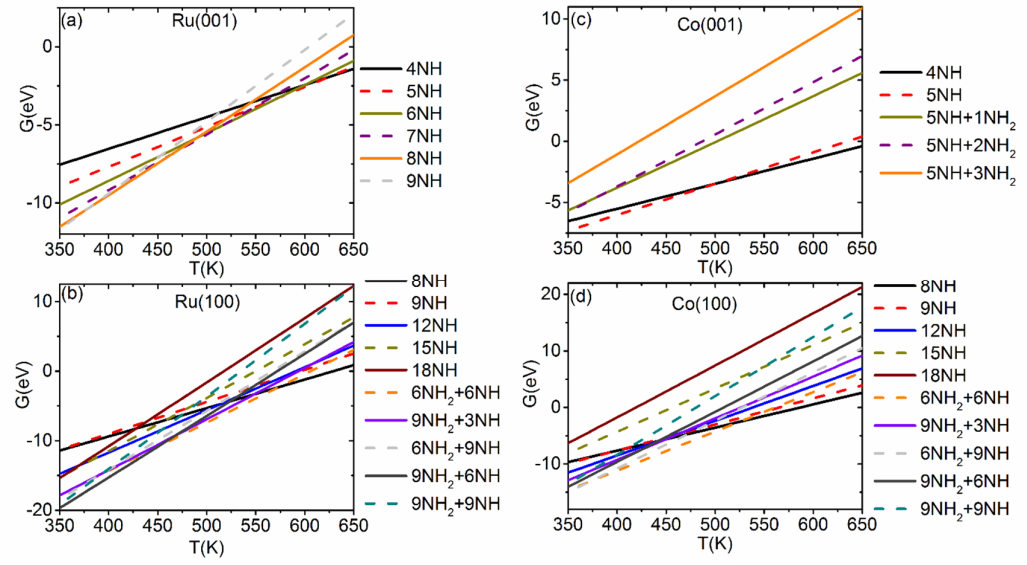

Figure 11. The plotted Gibbs free energy (ΔG) of NH_x with respect to operating temperature on Ru and Co surfaces. The pressure is set to be ultra-high vacuum (UHV) condition ($P/P^o = 5\times10^{-14}$).

For Ru (001), a surface terminated with high coverage, namely 8/9 ML – 1 ML NH coverage is the most stable in the typical ALD operating temperature range (350K-650K). On the Co (001) surface, a surface with a partial coverage of 5/9 ML NH dominates over the ALD operating temperature range between 400K and 650K. A Co (001) surface terminated with a mixture of NH and NH_2 (5NH and $2NH_2$) is only favorable at the lower temperature range between 350K and 400K.

Table 5. The preferred surface terminations of Ru and Co (001) and (100) surface as a functional of temperature under ALD operating condition

	Ru(3x3)	Co(3x3)
(001)	1ML NH (350K-550K); 8/9ML NH (550K-650K)	5NH_$2NH_2$ (350K-400K); 5/9ML NH (400K-650K)
(100)	$9NH_2$_9NH (350K-500K); $9NH_2$_6NH (500K-600K); $6NH_2$_6NH (600K-650K)	$9NH_2$_9NH (350K-375K); $6NH_2$_9NH (375K-550K); $6NH_2$_6NH (550K-650K)

On Ru (100) and Co (100) surfaces the fully covered 9NH and $9NH_2$ surface termination is most stable at low temperature. Upon increasing the temperature, NH (or NH_2) is first desorbed from surface so that the termination changes to 6NH and $9NH_2$ (or 9NH and $6NH_2$), whereby both terminations are essentially iso-energetic. Thereafter, NH_2 (or NH) desorbs to produce a surface terminated with 6NH and $6NH_2$ on Co and Ru (100) surfaces. The results are summarized in Table 5. Clearly, the nature of the NH_x terminated Co and Ru surfaces are

temperature dependent. This can affect the adsorption strength of the metal organic precursors ($RuCp_2$ and $CoCp_2$) and the following Cp ligand desorption process. We can see that the growth and thin film quality of Co and Ru will therefore be sensitive to the deposition temperature and a higher deposition temperature would result in lower coverages of NH/NH_2 for Co which could impact on film quality. Thus the use of lower temperature plasma should be beneficial in promoting growth of high quality metal films.

4. Conclusions

The stability of NH and NH_2 terminations of Co and Ru metal surfaces are investigated by first principle calculations as the starting point of simulating the PE-ALD process using N-plasma. The three most stable surfaces are (001), (101), and (100) and we choose the (001) surface, with the lowest surface energy, and the (100) surface, with high reactivity but lower stability to perform the analysis of NH_x stability. For termination with exclusively NH or NH_2, the (001) surface has a preference for NH at the hcp site while NH_2 prefers the bridge site. On the (100) surface, both NH and NH_2 prefer to bind on bridge site with channel bridge for NH and surface bridge for NH_2.

When increasing the coverage, on the (001) surface, the saturation coverage on Ru is 1 ML NH and 5/9 ML NH for Co. For NH_2 termination, the saturation coverages are 5/9 ML on both Co and Ru surfaces. The weaker NH-NH repulsion effect on Ru surface is attributed to larger surface area compared to the corresponding Co surface. Additionally, NH_2 is unstable at high coverage by desorbing from metal surface or dissociating into NH + H. On the (100) surface, the individual saturation coverages on the Ru and Co surfaces are the same, namely up to 2 ML for NH and 1 ML for NH_2.

On (001) surfaces, in a mixed termination mode, we start from the NH pre-covered surface model and add NH_2. On the (100) surfaces, an NH_2 pre-covered surface model is then modified by adding NH and NH_2. The results are analyzed with thermodynamics by calculating the Gibbs energy. Both the UHV condition and standard ALD operating condition are considered to elucidate the effect of pressure and temperature on the termination of metal surfaces. We find that under literature PE-ALD operating condition, with a temperature range of 350K-650K, and $P/P^o = 1.97\times10^{-6}$, the most stable NH_x terminated metal surfaces are 1 ML NH on Ru(001) (350K-550K), 5/9 ML NH on Co(001) surface (400K-650K) and a mixture of NH and NH_2 on both Ru (100) and Co (100) surfaces. This work provides new information on the stability of NH_x terminations of metal surfaces present after nitrogen plasma step in PE-ALD and is a starting point for the further investigation of the interaction with the corresponding metal precursors.

Acknowledgements

We acknowledge generous support from Science Foundation Ireland (SFI) through the SFI-NSFC Partnership program, Grant Number 17/NSFC/5279, NITRALD and the support of Prof. Zhang and Prof. Lu at Fudan. Computing resources have been generously supported by Science Foundation Ireland at Tyndall and through the SFI/HEA-funded Irish Center for High End Computing (www.ichec.ie).

References

(1) Qu, X.-P.; Tan, J.-J.; Zhou, M.; Chen, T.; Xie, Q.; Ru, G.-P.; Li, B.-Z. Improved barrier properties of ultrathin Ru film with TaN interlayer for copper metallization. *Appl. Phys. Lett.* **2006,** *88* (15), 151912.

(2) Greenslit, D. V.; Eisenbraun, E. Characterization of Ultrathin PEALD-Grown RuCo Films for Diffusion Barrier and Copper Direct-Plate Applications. *ECS Trans.* **2011,** *35* (20), 17.

(3) Chakraborty, T.; Eisenbraun, E. T. Microstructure analysis of plasma enhanced atomic layer deposition-grown mixed-phase RuTaN barrier for seedless copper electrodeposition. *J. Vac. Sci. Technol. A* **2012,** *30* (2), 020604.

(4) Miikkulainen, V.; Leskelä, M.; Ritala, M.; Puurunen, R. L. Crystallinity of inorganic films grown by atomic layer deposition: Overview and general trends. *J. Appl. Phys.* **2013,** *113* (2), 2.

(5) Van Bui, H.; Grillo, F.; Van Ommen, J. Atomic and molecular layer deposition: off the beaten track. *Chem. Commun.* **2017,** *53* (1), 45.

(6) Weber, M.; Julbe, A.; Ayral, A.; Miele, P.; Bechelany, M. Atomic layer deposition for membranes: Basics, challenges, and opportunities. *Chem. Mater.* **2018,** *30* (21), 7368.

(7) George, S. M. Atomic layer deposition: an overview. *Chem. Rev.* **2009,** *110* (1), 111.

(8) Bilousov, O. V.; Ren, Y.; Törndahl, T.; Donzel-Gargand, O.; Ericson, T.; Platzer-Björkman, C.; Edoff, M.; Hägglund, C. Atomic layer deposition of cubic and orthorhombic phase tin monosulfide. *Chem. Mater.* **2017,** *29* (7), 2969.

(9) Xie, Q.; Jiang, Y.-L.; Detavernier, C.; Deduytsche, D.; Van Meirhaeghe, R. L.; Ru, G.-P.; Li, B.-Z.; Qu, X.-P. Atomic layer deposition of TiO_2 from tetrakis-dimethyl-amido titanium or Ti isopropoxide precursors and H_2O. *J. Appl. Phys.* **2007,** *102* (8), 083521.

(10) Hu, Z.; Turner, C. H. Atomic layer deposition of TiO_2 from TiI_4 and H_2O onto SiO_2 surfaces: Ab initio calculations of the initial reaction mechanisms. *J. Am. Chem. Soc.* **2007,** *129* (13), 3863.

(11) Hu, Z.; Turner, C. H. Initial surface reactions of TiO_2 atomic layer deposition onto SiO_2 surfaces: density functional theory calculations. *J. Phys. Chem. B* **2006,** *110* (16), 8337.

(12) Somani, S.; Mukhopadhyay, A.; Musgrave, C. Atomic layer deposition of tantalum nitride using a novel precursor. *J. Phys. Chem. C* **2011,** *115* (23), 11507.

(13) Lim, B. S.; Rahtu, A.; Gordon, R. G. Atomic layer deposition of transition metals. *Nat. Mater.* **2003,** *2* (11), 749.

(14) Lu, J.; Elam, J. W.; Stair, P. C. Synthesis and stabilization of supported metal catalysts by atomic layer deposition. *Acc. Chem. Res.* **2013,** *46* (8), 1806.

(15) Kim, H.; Oh, I.-K. Review of plasma-enhanced atomic layer deposition: Technical enabler of nanoscale device fabrication. *Jpn. J. Appl. Phys.* **2014,** *53* (3S2), 03DA01.

(16) Elliott, S. D.; Dey, G.; Maimaiti, Y.; Ablat, H.; Filatova, E. A.; Fomengia, G. N. Modeling mechanism and growth reactions for new nanofabrication processes by atomic layer deposition. *Adv. Mater.* **2016,** *28* (27), 5367.

(17) Soethoudt, J.; Grillo, F.; Marques, E. A.; van Ommen, J. R.; Tomczak, Y.; Nyns, L.; Van Elshocht, S.; Delabie, A. Diffusion□mediated growth and size□dependent nanoparticle reactivity during ruthenium atomic layer deposition on dielectric substrates. *Adv. Mater. Interfaces* **2018,** *5* (24), 1800870.

(18) Ritala, M.; Kukli, K.; Rahtu, A.; Räisänen, P. I.; Leskelä, M.; Sajavaara, T.; Keinonen, J. Atomic layer deposition of oxide thin films with metal alkoxides as oxygen sources. *Science* **2000,** *288* (5464), 319.

(19) Shirazi, M.; Elliott, S. D. Multiple proton diffusion and film densification in atomic layer deposition modeled by density functional theory. *Chem. Mater.* **2013,** *25* (6), 878.

(20) Elliott, S.; Scarel, G.; Wiemer, C.; Fanciulli, M.; Pavia, G. Ozone-based atomic layer deposition of alumina from TMA: Growth, morphology, and reaction mechanism. *Chem. Mater.* **2006,** *18* (16), 3764.

(21) Puurunen, R. L. Surface chemistry of atomic layer deposition: A case study for the trimethylaluminum/water process. *J. Appl. Phys.* **2005,** *97* (12), 9.

(22) Sun, F.; Yu, J. C.; Wang, X. Construction of size-controllable hierarchical nanoporous TiO_2 ring arrays and their modifications. *Chem. Mater.* **2006,** *18* (16), 3774.

(23) Fomengia, G. N.; Nolan, M.; Elliott, S. D. First principles mechanistic study of self-limiting oxidative adsorption of remote oxygen plasma during the atomic layer deposition of alumina. *Phys. Chem. Chem. Phys.* **2018,** *20* (35), 22783.

(24) Raymand, D.; Van Duin, A. C.; Goddard III, W. A.; Hermansson, K.; Spångberg, D. Hydroxylation structure and proton transfer reactivity at the zinc oxide–water interface. *J. Phys. Chem. C* **2011,** *115* (17), 8573.

(25) Yuzawa, H.; Aoki, M.; Otake, K.; Hattori, T.; Itoh, H.; Yoshida, H. Reaction mechanism of aromatic ring hydroxylation by water over platinum-loaded titanium oxide photocatalyst. *J. Phys. Chem. C* **2012,** *116* (48), 25376.

(26) Fan, C.; Chen, C.; Wang, J.; Fu, X.; Ren, Z.; Qian, G.; Wang, Z. Black hydroxylated titanium dioxide prepared via ultrasonication with enhanced photocatalytic activity. *Sci. Rep.* **2015,** *5*, 11712.

(27) Novell-Leruth, G.; Valcarcel, A.; Pérez-Ramírez, J.; Ricart, J. M. Ammonia dehydrogenation over platinum-group metal surfaces: Structure, stability, and reactivity of adsorbed NHx species. *J. Phys. Chem. C* **2007,** *111* (2), 860.

(28) Novell-Leruth, G.; Valcarcel, A.; Clotet, A.; Ricart, J.; Perez-Ramirez, J. DFT characterization of adsorbed NH_x species on Pt (100) and Pt (111) surfaces. *J. Phys. Chem. B* **2005,** *109* (38), 18061.

(29) Logadottir, A.; Nørskov, J. K. Ammonia synthesis over a Ru (0001) surface studied by density functional calculations. *J. Catal.* **2003,** *220* (2), 273.

(30) Popa, C.; Offermans, W.; Van Santen, R.; Jansen, A. Ab initio density-functional theory study of NH_x dehydrogenation and reverse reactions on the Rh (111) surface. *Phys. Rev. B* **2006,** *74* (15), 155428.

(31) Kim, J.-M.; Lansalot, C.; Dussarrat, C.; Gatineau, J.; Kim, H. Plasma-enhanced atomic layer deposition of cobalt using cyclopentadienyl isopropyl acetamidinato-cobalt as a precursor. *Jpn. J. Appl. Phys.* **2010,** *49* (5S2), 05FA10.

(32) Vos, M. F.; van Straaten, G.; Kessels, W. E.; Mackus, A. J. Atomic layer deposition of cobalt using H_2-, N_2-, and NH_3-based plasmas: on the role of the Co-reactant. *J. Phys. Chem. C* **2018,** *122* (39), 22519.

(33) Kim, H. High-quality cobalt thin films by plasma-enhanced atomic layer deposition. *Electrochem. Solid State Lett.* **2006,** *9* (11), G323.

(34) Kim, S. K.; Lee, S. Y.; Lee, S. W.; Hwang, G. W.; Hwang, C. S.; Lee, J. W.; Jeong, J. Atomic layer deposition of Ru thin films using 2, 4-(dimethylpentadienyl)(ethylcyclopentadienyl) Ru by a liquid injection system. *J. Electrochem. Soc.* **2007,** *154* (2), D95.

(35) Leick, N.; Verkuijlen, R.; Lamagna, L.; Langereis, E.; Rushworth, S.; Roozeboom, F.; Van de Sanden, M.; Kessels, W. Atomic layer deposition of Ru from $CpRu(CO)_2Et$ using O_2 gas and O_2 plasma. *J. Vac. Sci. Technol. A* **2011,** *29* (2), 021016.

(36) Klesko, J. P.; Kerrigan, M. M.; Winter, C. H. Low temperature thermal atomic layer deposition of cobalt metal films. *Chem. Mater.* **2016,** *28* (3), 700.

(37) Zhu, B.; Ding, Z.-J.; Wu, X.; Liu, W.-J.; Zhang, D. W.; Ding, S.-J. Plasma-enhanced atomic layer deposition of cobalt films using $Co(EtCp)_2$ as a metal precursor. *Nanoscale Res. Lett.* **2019,** *14* (1), 76.

(38) Shimizu, H.; Sakoda, K.; Momose, T.; Koshi, M.; Shimogaki, Y. Hot-wire-assisted atomic layer deposition of a high quality cobalt film using cobaltocene: Elementary reaction analysis on NHx radical formation. *J. Vac. Sci. Technol. A* **2012,** *30* (1), 01A144.

(39) Yoon, J.; Kim, D.; Cheon, T.; Kim, S.-H.; Kim, H. Atomic layer deposition of Co using N_2/H_2 plasma as a reactant. *J. Electrochem. Soc.* **2011,** *158* (11), H1179.

(40) Elliott, S. D.; Dey, G.; Maimaiti, Y. Classification of processes for the atomic layer deposition of metals based on mechanistic information from density functional theory calculations. *J. Chem. Phys.* **2017,** *146* (5), 052822.

(41) Zydor, A.; Elliott, S. D. $TiCp^*(OMe)_3$ versus $Ti(OMe)_4$ in atomic layer deposition of TiO_2 with water—Ab initio modelling of atomic layer deposition surface reactions. *J. Nanosci. Nanotechnol.* **2011,** *11* (9), 8089.

(42) Shirazi, M.; Elliott, S. D. Atomistic kinetic Monte Carlo study of atomic layer deposition derived from density functional theory. *J. Comput. Chem.* **2014,** *35* (3), 244.

(43) Lim, J.-W.; Park, J.-S.; Kang, S.-W. Kinetic modeling of film growth rates of TiN films in atomic layer deposition. *J. Appl. Phys.* **2000,** *87* (9), 4632.

(44) Phung, Q. M.; Pourtois, G.; Swerts, J.; Pierloot, K.; Delabie, A. Atomic layer deposition of ruthenium on ruthenium surfaces: A theoretical study. *J. Phys. Chem. C* **2015,** *119* (12), 6592.

(45) Phung, Q. M.; Vancoillie, S.; Pourtois, G.; Swerts, J.; Pierloot, K.; Delabie, A. Atomic layer deposition of Ruthenium on a titanium nitride surface: A density functional theory study. *J. Phys. Chem. C* **2013,** *117* (38), 19442.

(46) Kresse, G.; Joubert, D. From ultrasoft pseudopotentials to the projector augmented-wave method. *Phys. Rev. B* **1999,** *59* (3), 1758.

(47) Perdew, J. P.; Chevary, J. A.; Vosko, S. H.; Jackson, K. A.; Pederson, M. R.; Singh, D. J.; Fiolhais, C. Atoms, molecules, solids, and surfaces: Applications of the generalized gradient approximation for exchange and correlation. *Phys. Rev. B* **1992,** *46* (11), 6671.

(48) Perdew, J. P.; Burke, K.; Ernzerhof, M. Generalized gradient approximation made simple. *Phys. Rev. Lett.* **1996,** *77* (18), 3865.

(49) Monkhorst, H. J.; Pack, J. D. Special points for Brillouin-zone integrations. *Phys. Rev. B* **1976,** *13* (12), 5188.

(50) Henkelman, G.; Uberuaga, B. P.; Jónsson, H. A climbing image nudged elastic band method for finding saddle points and minimum energy paths. *J. Chem. Phys.* **2000,** *113* (22), 9901.

(51) Zhang, C.; Lynch, M.; Hu, P. A density functional theory study of stepwise addition reactions in ammonia synthesis on Ru (0001). *Surf. Sci.* **2002,** *496* (3), 221.

(52) Zhao, P.; He, Y.; Cao, D.-B.; Wen, X.; Xiang, H.; Li, Y.-W.; Wang, J.; Jiao, H. High coverage adsorption and co-adsorption of CO and H_2 on Ru (0001) from DFT and thermodynamics. *Phys. Chem. Chem. Phys.* **2015,** *17* (29), 19446.

Table of Content Graphic

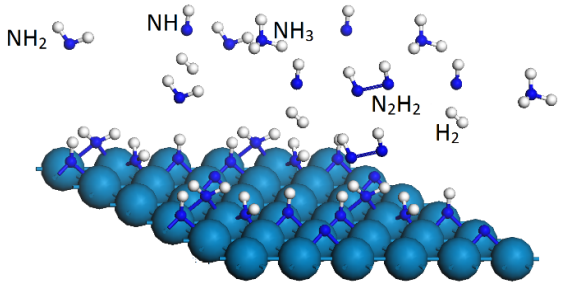

Ru or Co (001) surfaces

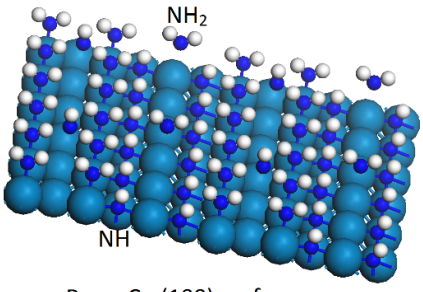

Ru or Co (100) surfaces